Pyridoxal based ONS and ONO vanadium(V) complexes: Structural analysis and catalytic application in organic solvent free epoxidation

Jana Pisk, Jean-Claude Daran, Rinaldo Poli, Dominique Agustin

Pyridoxal based *ONS* and *ONO* vanadium(V) complexes: structural analysis and catalytic application in organic solvent free epoxidation.

Jana Pisk,[†,‡,§,¶], Jean-Claude Daran,[†, ¶] Rinaldo Poli,[†, ¶, ǁ] Dominique Agustin*[‡, §, ¶]

[†] CNRS; LCC (Laboratoire de Chimie de Coordination); Université de Toulouse; UPS, INPT, 205, route de Narbonne, F-31077 Toulouse, France.

[‡] University of Zagreb, Faculty of Science, Department of Chemistry, Division of General and Inorganic Chemistry, Horvatovac 102 a, 10000 Zagreb, Croatia.

[§] Institut Universitaire de Technologie Paul Sabatier, Département de Chimie, Av. Georges Pompidou, BP 20258, F-81104 Castres Cedex, France.
Email: dominique.agustin@iut-tlse3.fr.

[¶] Université de Toulouse, UPS, INPT, F-31077 Toulouse Cedex 4, France.

[ǁ] Institut Universitaire de France, 103, bd Saint-Michel, F-75005 Paris, France.

Abstract

A series of dinuclear and mononuclear oxovanadium(V) complexes containing tridentate Schiff base ligands derived from pyridoxal and appropriate thiosemicarbazide or hydrazide are reported. The compounds were characterised by elemental analysis, thermogravimetric analysis, IR and NMR spectroscopy. The molecular structure of the dioxido-vanadium(V) complex $[VO_2(HL^5)]\cdot MeOH\cdot H_2O$ (H_2L^5 = pyridoxal benzhydrazido ligand), determined by X-ray crystallography, reveals an unexpected distorted trigonal bipyramidal arrangement of the VO_2 moiety. A DFT study of this molecule and of the related $[VO_2(H_2L^5)]$ complex of V^{IV} reveals a moderate effect of the oxidation state change on the bond distances and angles, pointing to solvation as the cause of the structural distortion. All complexes were tested as (pre)catalysts for olefin epoxidation by aqueous *tert*-butylhydroxyperoxide (TBHP) under solvent-free conditions. Low vanadium loadings (0.05% *vs*. olefin) resulted in good cyclooctene conversions and TOFs. The lifetime of one catalyst was explored through repeated runs with recovery/recycling. DFT calculations have also addressed the olefin epoxidation mechanism, which reveals the possible direct O atom transfer from the activated *tert*-butoxido (tBuOO$^-$) ligand, without the need to generate a peroxido (O_2^{2-}) ligand.

Keywords: Vanadium(V) complexes / Pyridoxal Schiff base / Epoxidation mechanism / Solvent free / Catalyst recovery / DFT calculations

Graphical Abstract

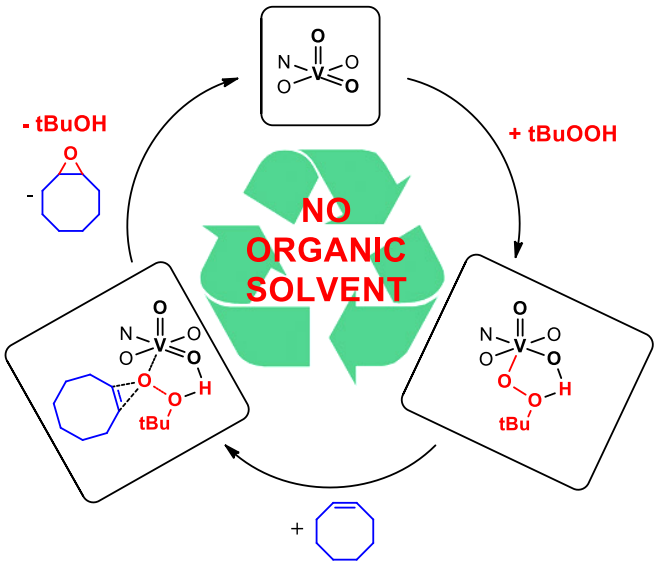

Highlights

- New vanadium complexes have been synthesized and characterized
- Their catalytic activity was studied under solvent-free conditions.
- DFT calculations clarify the mechanism of the catalytic cycle

1. Introduction

Vanadium has growing impact in coordination chemistry because of its biological and catalytic properties [1]. It can exist in wide range of oxidation states from –III to +V [2]. The rich chemistry of oxidovanadium(V) is due to its ability to adopt three different structural motifs: i) $[VO]^{3+}$, ii) $[VO_2]^{+}$ and iii) $[V_2O_3]^{4+}$ [3].The combination of the pyridoxal moiety with thiosemicarbazides and hydrazides provides interesting chemical and biological activity for the resulting condensation products. It is known that the neutral form of such ligands, H_2L, exists in three tautomeric forms **A-C** (scheme 1), of which the third one is zwitterionic. The singly and doubly deprotonated forms HL^- and L^{2-} have also been described and it has been demonstrated that their tridentate coordination involves the limiting forms shown in scheme 1 [4]. Oxido vanadium metal complexes with Schiff base chelating ligands have been reported [5] in which *O*, *N* donor ligands have the tendency to stabilize vanadium in its highest oxidation state.

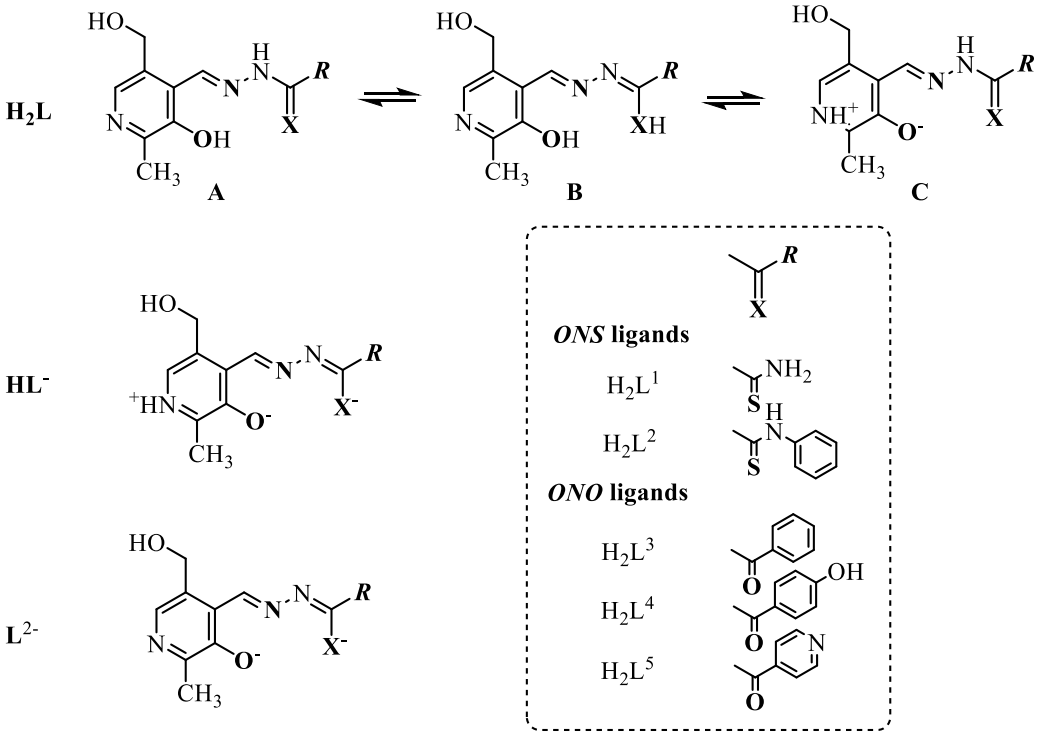

Scheme 1. *ONS* and *ONO* donors ligands used for the preparation of vanadium^{V} complexes. The ligand tautomerism is also illustrated in the scheme.

Coordination complexes of oxidovanadium(V) $[VO]^{3+}$ and dioxidovanadium(V) $[VO_2]^{+}$ are well known as (pre)catalysts for oxidation reactions of different substrates [6] as well as in

sulfoxidation processes [7], but only few studies concern olefin epoxidation [8]. Epoxides are important intermediates for the synthesis of several commercial products [9]. Traditional catalytic processes use organic solvents, which cause safety and pollution problems due to flammability, toxicity and volatility [10]. Avoiding solvents is the crucial point for "greening" the epoxidation processes. Following the principle *"the best solvent is no solvent"* [11], an organic solvent-free process is emerging as the most appropriate choice, since it is environmentally friendlier, less hazardous and characterized by lower running costs [10-12]. Taking into account economic and environmental viewpoints, great efforts are invested in catalyst recovery and recycling [8g,13]. Although the catalytic efficiency is usually significantly decreased in repeated runs, the opposite trend (activity increase in subsequent runs) may also be observed [14].

We present herein the preparation and spectroscopic characterisation of mononuclear and dinuclear vanadium (V) complexes derived from the ligands H_2L^1 – H_2L^5 (Scheme1), of general formula $[V_2O_3(L^1)_2]$, $[V_2O_3(HL^1)_2]Cl_2$, $[V_2O_3(L^2)_2]\cdot 2MeOH$, $[V_2O_3(HL^2)_2]Cl_2\cdot 2MeOH$, $[VO_2(HL^{3,4})]\cdot MeOH\cdot H_2O$, and $[VO_2(HL^5)]$ (Scheme 2). All isolated species were used as (pre)catalysts for the organic solvent-free epoxidation of *cis*-cyclooctene using the same procedure of our previously published studies with the vanadium complex $[V_2O_3(SAP)_2]$ (SAP = salicylideneaminophenolato) [8c], with the Keggin polyoxometalate $[PMo_{12}O_{40}]^{3-}$ [15],with the molybdenum complex $[MoO_2(SAP)]_2$ [16], and in particular with tridentate pyridoxal derivatives of dioxidomolybdenum(VI) [17]. In these epoxidations, the oxidant is *tert*-butylhydroperoxide (TBHP) administered as an aqueous solution, water not acting as a reaction solvent. Moreover, the lifetime of $[VO_2(HL^4)]\cdot MeOH\cdot H_2O$ catalyst was explored through repeated runs with recovery/recycling. The olefin epoxidation mechanism has also been addressed by DFT calculations.

2. Experimental Section

2.1. Materials and methods:

Pyridoxal hydrochloride, thiosemicarbazides, hydrazides, isoniazide, [$VO(acac)_2$], aqueous TBHP (70%), cyclooctene and acetophenone were commercially available (Aldrich) and used as received. Solvents (MeOH, EtOH, Et_2O) were reagent grade. All the ligands were prepared according to literature procedures [18,19]. Infrared spectra were recorded on KBr pellets at room temperature with a Mattson Genesis II FTIR spectrometer. Thermogravimetric analyses were performed with a thermal analyzer SDT-Q600. The samples were placed into platinum crucibles and heated at 10 K min^{-1} in reconstituted air flow from 25 °C to 600 °C. ^1H NMR spectra were recorded at 200.1 MHz on a Bruker Advance DPX-200 spectrometer. ^{51}V NMR spectra were recorded at 131.6 MHz on a Bruker Avance 500 spectrometer. Elemental analyses (C, H, N) were performed by the Laboratoire de Chimie de Coordination analytical service. The catalytic reactions were followed by gas chromatography (GC) on an Agilent 6890A chromatograph equipped with FID detector and a DB5-MS capillary column (30 m x 0.32 mm x 0.25 µm). The GC parameters were quantified with authentic samples of the reactants and products. The conversion of *cis*-cyclooctene (COE) Conversion = [$n(COE_{consumed})/n(COE_{introduced})$]×100 and the selectivity towards cyclooctene oxide (COEO) Selectivity = [$n(COEO_{formed})/n(COE_{consumed})$]×100 were calculated only from the organic phase from GC calibration curves ($r^2 = 0.999$).

2.2. Synthesis of µ-oxido bis oxidovanadium complexes

A mixture of [$VO(acac)_2$] (0.05 g, 0.2 mmol) and the appropriate ligand (H_2L^1, H_2L^1·HCl, H_2L^2, H_2L^2·HCl) (0.2 mmol) in the appropriate alcohol (20 mL) was refluxed for four hours. The precipitate formed during the reaction was filtered, washed with alcohol, and dried. For all ^1H NMR spectra, the pyridoxal CH_3 resonance, which should appear around 2.5 ppm, was not visible because of overlap with the DMSO signal.

Complex [$V_2O_3(L^1)_2$] (**1**). Dark greenish-black product obtained from EtOH. Yield: 0.04 g, 64%. Found: C, 34.48; H, 3.46; N, 17.34%. $C_{18}H_{20}N_8O_7S_2V_2$ requires C, 34.53; H, 3.22; N, 17.89%.

TGA: 27.5% V_2O_5 residue (requires 29.0%). IR(KBr): ν/cm^{-1} 1616, 1575 (C=N), 1330 (C–O), 970 (V=O), 773 (V–O–V), 623 (C–S). ^1H NMR (DMSO-d_6): 4.77 (m, 2H, CH_2), 5.60 (m,

1H, OH), 7.35 (m, 2H, NH_2), 7.94 (m, 1H, CH_{arom}), 8.86 (s, 1H, CH=N). ^{51}V NMR (DMSO-d_6) -456.7.

Complex $[V_2O_3(HL^1)_2]Cl_2$ (**2**). Black product obtained from EtOH. Yield: 0.05 g, 72%. Found: C, 30.14; H, 3.20; N, 15.84; Cl, 9.24%. $C_{18}H_{22}N_8Cl_2O_7S_2V_2$ requires C, 30.93; H, 3.17; N, 16.02; Cl, 10.14%.

TGA: 25.7% V_2O_5 residue (requires 26.0%). IR (KBr): ν/cm^{-1} 1617, 1567 (C=N), 1340 (C–O), 968 (V=O), 781 (V–O–V), 617 (C–S). ^{1}H NMR (DMSO-d_6): 4.81 (m, 2H, CH_2), 5.34 (m, 1 H, OH), 7.50 (m, 2H, NH_2), 8.03 (m, 1H, CH_{arom}), 8.85 (s, 1H, CH=N),). ^{51}V NMR (DMSO- d_6) -457.3.

Complex $[V_2O_3(L^2)_2]$·2MeOH (**3**). Dark brown product obtained from MeOH. Yield: 0.05 g, 59%. Found: C, 45.24; H, 3.94; N, 13.46%. $C_{32}H_{36}N_8O_9S_2V_2$ requires C, 45.62; H, 4.31; N, 13.30%.

TGA: 6.8% MeOH loss (requires 7.4%); 21.6% V_2O_5 residue (requires 21.6%). IR(KBr): ν/cm^{-1}1616, 1577 (C=N), 1319 (C–O), 960 (V=O), 758 (V–O–V), 625 (C–S). ^{1}H NMR (DMSO-d_6): 4.89 (m, 2H, CH_2), 5.70 (m, 1 H, OH), 7.06 (m, 1H, CH_{ar}), 7.36 (m, 2H, CH_{ar}), 7.87 (m, 2H, CH_{ar}), 8.03 (m, 1H, CH_{ar}), 9.13 (s, 1H, CH=N), 9.88 (s, 1H, NH). ^{51}V NMR (DMSO- d_6) -466.9.

Complex $[V_2O_3(HL^2)_2]Cl_2$·2MeOH (**4**). Dark greenish-brown product obtained from MeOH. Yield: 0.08 g, 83%. Found: C, 41.54; H, 4.14; N, 11.94; Cl, 7.34%. $C_{32}H_{38}N_8Cl_2O_9S_2V_2$ requires C, 41.99; H, 4.18; N, 12.24; Cl, 7.75%

. TGA: 4.3% MeOH loss (requires 6.7%); 17.1% V_2O_5 residue, (requires 19.9%). IR(KBr): ν/cm^{-1}1598, 1571 (C=N), 1319 (C–O), 960 (V=O), 744 (V–O–V), 623 (C–S).^{1}H NMR (DMSO-d_6): 4.94 (m, 2H, CH_2), 5.80 (m, 1H, OH), 7.08 (m, 1H, CH_{ar}), 7.42 (m, 2H, CH_{ar}), 7.65 (m, 1H, NH^+), 7.89 (m, 2H, CH_{ar}), 8.12 (m, 1H, CH_{arom}), 9.12 (s, 1H, CH=N), 9.93 (s, 1H, NH). ^{51}V NMR (DMSO- d_6) -465.3.

2.3. Synthesis of dioxidovanadium complexes:

A mixture of $[VO(acac)_2]$ (0.05 g, 0.2 mmol) and the appropriate ligand (0.2 mmol) in methanol (20 mL) was refluxed for 4 h and the precipitate formed during the reaction was filtered, washed with methanol and dried.

Complex [$VO_2(HL^3)$]·MeOH·H_2O (**5**). Yellow crystals. Yield: 0.02 g, 24%. Found: C, 45.74; H, 4.91; N, 9.74%. $C_{16}H_{20}N_3O_7V$ requires C, 46.06; H, 4.83; N, 10.07%.

TGA: 12.8% MeOH+H_2O loss, (requires 12.0%); 21.8% V_2O_5 residue (requires 21.7%). IR(KBr): ν//cm^{-1} 1617 (C=N), 933, 916 (O=V=O). ^{1}H NMR (DMSO-d_6): 2.56 (m, CH_3), 4.89 (m, 2H, CH_2), 5.70 (m, 1H, OH), 7.50-7.57 (m,3H, CH_{ar}), 8.00 (s,1H, CH_{ar}), 8.07-8.09 (m,2H, CH_{ar}), 8.28 (1H, CH=N). ^{51}V NMR (DMSO- d_6) -536.2. Slow evaporation of the methanol solution led to the isolation of single crystals suitable for a structural determination through X-ray crystallography.

Complex [$VO_2(HL^4)$]·MeOH·H_2O (**6**). Orange product. Yield: 0.03 g, 38%. Found: C, 43.94; H, 4.44; N, 9.88%. $C_{16}H_{20}N_3O_8V$ requires C, 44.36; H, 4.65; N, 9.70%.

TGA: 9.2% MeOH+H_2O loss (requires 11.5%); 22.4% V_2O_5 residue (requires 21.0%). IR(KBr): ν//cm^{-1}1616 (C=N), 941, 921 (O=V=O). ^{1}H NMR (DMSO-d_6): 2.80 (m, CH_3), 4.83 (m, 2H, CH_2), 5.70 (m, 1H, OH), 6.88 (m,2H, CH_{ar}), 7.99 (3H, CH_{ar}), 9.25 (1H, CH=N), 10.14 (m,1H, NH^+). ^{51}V NMR (DMSO- d_6) -536.1.

Complex [$VO_2(HL^5)$] (**7**). Complex **7** was prepared according to the previously published method[1d] with the exception of using directly [$VO(acac)_2$] and HL^5 ligand in methanol.

Dark yellow product. Yield: 0.03 g, 41%. Found: C, 45.54; H, 3.77; N, 14.84%. $C_{14}H_{13}N_4O_5V$ requires C, 45.67; H, 3.56; N, 15.21%.

TGA: 26.9 % V_2O_5 residue (requires 24.7%). IR(KBr): ν//cm^{-1} 1596 (C=N), 1257 (C–O), 954, 901 (O=V=O). ^{1}H NMR (DMSO-d_6): 2.12 (m, CH_3), 4.85 (m, 2H, CH_2), 5.74 (m, 1H, OH), 7.95 (3H, CH_{ar}), 8.75 (2H, CH_{ar}), 9.36 (1H, CH=N). ^{51}V NMR (DMSO- d_6) -536.1.

2.4. Catalytic tests

Procedure A: A mixture of cyclooctene (2.76 mL, 20 mmol), acetophenone (internal reference) and V^V (pre)catalyst (0.01 mmol of V) was stirred and heated up to 80 °C before the addition of aqueous TBHP (70%, 5.48 mL, 40 mmol). The reaction was followed for 5 h by withdrawing aliquots at required times. During the kinetic study, 0.1 mL samples of the organic phase were taken from the reaction medium and mixed with 2 mL of Et_2O. A small quantity of MnO_2 was added to each sample in order stop the reaction by destroying the

remaining peroxide before analysis. The mixture was filtered through silica and analyzed by GC.

Procedure B: The procedure B is identical to the procedure A with 2 mg of solid recovered from procedure A using complex **6**.

Procedure C: The procedure C is identical to procedure A with 1 mg of solid recovered from procedure B.

Procedure D: The procedure D is identical to procedure A with use of 0.05 mol of complex **6**.

2.5. DFT Calculations

All calculations were carried out with the GAUSSIAN 03 program suite [20],within the DFT approach using the B3LYP three-parameter functional [21] in conjunction with the 6-31 G** basis set for the light atoms (O, N, C, H) plus the SDD set for the V atom, which includes a pseudopotential, augmented by an *f* polarization function with the optimized [22] 1.715 coefficient. The geometry of $[VO_2(HL^3)]$ was optimized from the geometry determined by X-ray diffraction without any symmetry constraint. The optimized geometries of all stable compounds and reaction intermediates were confirmed to be local minima by the frequencies analysis. Likewise, the frequency analysis confirmed the nature of the optimized transition states as first order saddle points (only one imaginary frequency at –439.18i for TS II and at –514.55i for TS III corresponding to the expected reaction coordinates). Thermochemical corrections were obtained at 298.15 K on the basis of frequency calculations, using the standard approximations (ideal gas, rigid rotor and harmonic oscillator).

2.6. X-Ray Crystallographic Study

A single crystal of the compound **5** was mounted under inert perfluoropolyether on the tip of a loop and cooled in the cryostream of an Agilent Technologies GEMINI extra diffractometer with an EOS CCD detector. Data were collected using the monochromatic Mo Kα radiation (λ = 0.71073 Å). The structure was solved by direct method (SIR97) [23] and refined by least-squares procedures on F^2 using SHELXL-97 [24]. All H atoms attached to the C, N and O atoms were introduced at idealised positions and treated as riding on their parent atoms in

the calculations. Owing to the fact that the hydroxyl oxygen is located on the mirror plane, the H atom attached to it is statistically distributed over two symmetry related positions. The O atom of the water molecule is also located on the mirror plane and so the H atoms are symmetrically related to this plane. The methanol solvate is statistically disordered over two positions related through the mirror plane with the C atom located on the mirror. The drawing of the molecules was realised with the help of ORTEP3 [25]. Crystal data and refinement parameters are shown in Table 1. Crystallographic data (excluding structure factors) have been deposited with the Cambridge Crystallographic Data Centre as supplementary publication no. CCDC 977949. Copies of the data can be obtained free of charge on application to the Director, CCDC, 12 Union Road, Cambridge CB2 1EZ, UK (fax: (+44) 1223-336-033; e-mail: deposit@ccdc.cam.ac.uk).

Table 1. Crystal data and structure refinement for the complex **5**.

Empirical formula	$C_{16}H_{19}N_3O_7V$
Formula weight	416.28
Temperature	180(2) K
Wavelength	0.71073 Å
Crystal system	Orthorhombic
Space group	*Pnma*
Unit cell parameters	
a (Å)	19.5940(7)
b (Å)	6.6639(3)
c (Å)	13.6590(5)
Volume (Å^3)	1783.49(12)
Z	4
ρ_{calcd} (g cm^{-3})	1.550
μ (mm^{-1})	0.602
F(000)	860
Crystal size (mm^3)	0.66 x 0.037 x 0.026
θ range for data collection (°)	3.64 – 26.36
Reflections collected	10261
Reflections independent	1975 [*R*(int) = 0.0513]
Completeness to θ_{max} (%)	99.6
Absorption correction	Multiscan
Max. and min. transmission	1.0 and 0.946
Refinement method	Full–matrix least–squares on F^2
Data / restraints / parameters	1975 / 0 / 165
Goodness–of–fit on F^2	0.871
Final *R* indices [$I>2\sigma(I)$]	R_1 = 0.0324, wR_2 = 0.0669
R indices (all data)	R_1 = 0.0604, wR_2 = 0.0705
Largest diff. peak and hole	0.288 and –0.359 e.Å^{-3}

3. Results and Discussion

3.1. Synthesis and vibrational properties of vanadium(V) complexes

All vanadium(V) complexes were prepared by the reaction of the appropriate pyridoxal thiosemicarbazone or hydrazone ligand H_2L (Scheme 1) or the thiosemicarbazone hydrochloride analogue $H_2L{\cdot}HCl$ and $[VO(acac)_2]$ in refluxing methanol or ethanol, conditions that gave the best yield and the highest degree of purity for the products. At variance with the previously reported procedures that employed the potassium salts of H_2L^1, H_2L^3 and H_2L^5 [18,26], our syntheses made direct use of the neutral ligands. The IR spectra of complexes **1-4** exhibit sharp bands in the 960-970 cm^{-1} range and a band around 745-774 cm^{-1}. On the other hand, complexes **5-7** display two bands around 934-955 cm^{-1} and 900-916 cm^{-1}. As reported in the literature, bands in the 960-970 cm^{-1} region are assigned to ν(V=O), while those around 745-774 cm^{-1} correspond to ν(V–O–V), typical for binuclear compounds [11, 39b] . The bands observed in the spectra of complexes **5-7** correspond to the ν_a(O=V=O) and ν_s(O=V=O) vibrational modes, indicating mononuclear compounds [27, 39d]. For all the complexes, the stretching frequencies attributed to the *ONO* or *ONS* ligands are found around 1610 and 1570 cm^{-1} (C=N), around 1310 cm^{-1} (C–O) and around 620 cm^{-1} (C–S), in agreement with the literature data [18, 28]. The broad absorptions in the 3000-2600 cm^{-1} range, appearing in the spectra of the mononuclear dioxidovanadium(V) complexes, confirm the presence of the pyridinium moiety of HL^- [4, 17, 29].

The proposed structures of complexes **1-7** are presented in Scheme 2. All reactions probably lead initially to air-unstable $[V^{IV}(O)L]$ intermediates which convert to the final V(V) products in air, as previously proposed for other similar systems [18, 19]. The sulphur containing ligands H_2L^1 and H_2L^2 yield dinuclear neutral complexes where the dianionic $(L^1)^{2-}$ and $(L^2)^{2-}$ bind the central $[V_2O_3]^{4+}$ core in a tridentate *ONS* coordination mode, as already observed in other species.[18, 19] Use of the corresponding hydrochlorides, $H_2L^1{\cdot}HCl$ and $H_2L^2{\cdot}HCl$, yields the same structural motif with $(HL^1)^-$ and $(HL^2)^-$ ligands (*i.e.* **2** and **4**) where the ligand is still bonded in a tridentate *ONS* fashion and the additional proton is located on the pyridine N atom. However, the reaction does not proceed in the same manner with the *ONO* ligands $H_2L^{3\text{-}5}$, leading instead to the formation of mononuclear zwitterionic $[VO_2(HL)]$ complexes where the residual proton on the tridentate *ONO* ligand is again located on the pyridine N atom (scheme 2). Complexes **5** and **6** crystallized in the form of solvates with one MeOH and one H_2O molecule per vanadium complex, **5**·MeOH·H_2O and **6**·MeOH·H_2O.

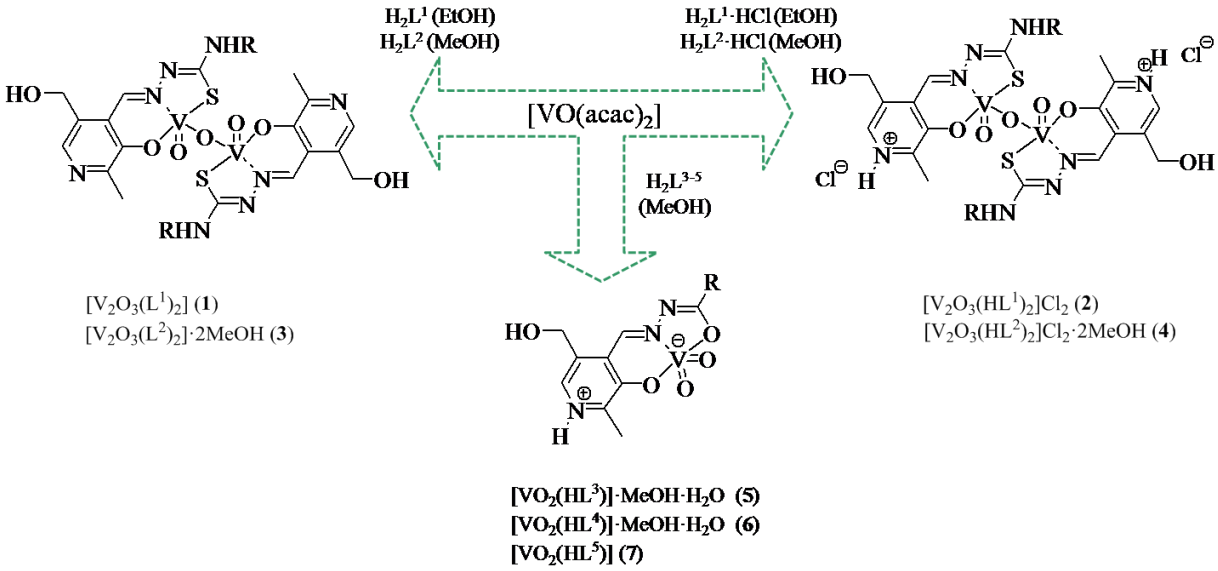

Scheme 2. Proposed compositions of V^V complexes.

2.2. NMR studies

The ^{1}H NMR spectra of compounds **1-7** in d^6-DMSO showed broad signals corresponding to the coordinated ligands, at sufficiently different positions from those of the free ligands. The spectra of compounds **3-6** showed signals corresponding to free methanol. For **3-4**, this is liberated by substitution, since DMSO is a stronger coordinating agent. The observation of the MeOH resonances for compounds **5** and **6** confirms the stoichiometry resulting from the thermal analysis.

Further analyses were carried out by ^{51}V NMR [30]. The two different chemical environments give ^{51}V NMR resonances in distinct chemical shift regions. Thus, all the complexes with *ONS* ligands exhibit a resonance between -456 and -470 ppm, in strict accordance with similar complexes and with the postulated coordination mode [18, 31]. On the other hand, all the *ONO* complexes exhibit resonances around -536 ppm, also corresponding to our structural assignment in relation to similar compounds.[19] Al these ^{51}V NMR data clearly indicate that all complexes contain vanadium (V).

3.2. Thermal analyses

When complexes **1-2** are heated in air, decomposition occurs in the 197 – 468 °C (**1**) and 164 – 525 °C (**2**) range, formally leading to two losses of (L^1–O) (or (L^1HCl–O) for **2** with

oxygen uptake from moisture and formation of V_2O_5. For complexes **3**-**4**, the first mass loss in the range 47 – 132 °C (**3**) and 40 – 105 °C (**4**) corresponds to the facile loss of the methanol molecules. In a second step, the ligand loss occurs at 200 – 480 °C (**3**) and 185 – 505 °C (**4**), resulting in the formation of V_2O_5. The dioxidovanadium complexes **5** and **6** behave in the same way, with a first desolvation step (methanol and water) in the 48 – 103 °C (**5**) and 42 – 124 °C (**6**) range followed by ligand loss leading to V_2O_5 in the 190 – 443 °C (**5**) and 175 – 470 °C (**6**) range. The complex **7**, which is non solvated, exhibits only the decomposition step to V_2O_5 in the 162 – 475 °C range.

3.3. X-ray structure

The structure of **5** was determined unambiguously by single crystal X-ray diffraction (Figure 1). The molecule is composed of a $[VO_2]^+$ fragment linked to the $(HL^3)^-$ ligand through *ONO* coordination. Relevant distances and angles are listed in Table 2.

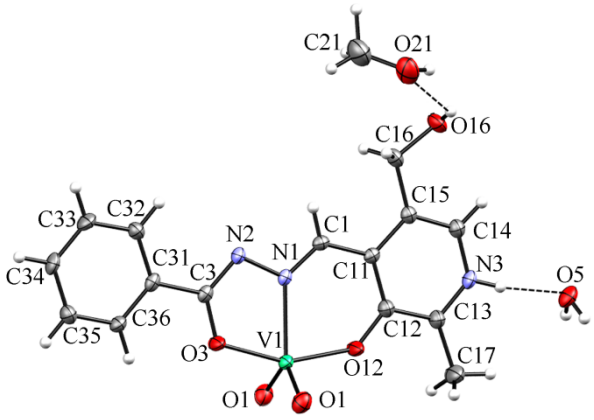

Figure 1. ORTEP View of the complex **5** $[VO_2(HL^3)]\cdot MeOH\cdot H_2O$. The ellipsoids are drawn at the 30% probability level. Hydrogen bonds between the complex and methanol and water molecules are represented by dotted lines.

Table 2. Selected bond lengths (Å) and interatomic angles (°) for the compound **5**.

Bond lengths			
V(1)–O(1)	1.6191(14)	V(1)–O(3)	1.950(2)
V(1)–O(12)	1.913(2)	V(1)–N(1)	2.153(2)
O(3)–C(3)	1.302(3)	C(12)–C(13)	1.414(4)

O(12)–C(12)	1.300(3)	O(16)–C(16)	1.427(3)
N(1)–C(1)	1.295(3)	C(1)–C(11)	1.435(4)
N(1)–N(2)	1.398(3)	C(3)–C(31)	1.478(4)
N(2)–C(3)	1.302(3)	C(11)–C(12)	1.410(4)
N(3)–C(13)	1.321(3)	C(11)–C(15)	1.420(4)
N(3)–C(14)	1.351(3)	C(21)–O(21)	1.383(4)

Interatomic angles

O(1)–V(1)–O(1i)	109.52(11)	O(1)–V(1)–N(1)	125.03(5)
O(1)–V(1)–O(12)	97.93(6)	O(12)–V(1)–N(1)	82.02(8)
O(1)–V(1)–O(3)	96.08(6)	O(3)–V(1)–N(1)	73.56(8)
O(12)–V(1)–O(3)	155.58(9)		

The geometry around the vanadium atom can best be described as distorted trigonal bipyramidal, the axial vector O(3)–V(1)–O(12) being distorted from linearity by the constraints of the tridentate *ONO* ligand. The angles between the equatorial ligands are close to 120°. All the heavy atoms of the complex are located on the (x, ¾, y) mirror plane except for the terminal O atoms, which are symmetrically located on each side of the plane. The O atom of the interstitial water molecule is located on the same mirror plane and acts as a hydrogen bond donor through two H atoms and as a hydrogen bond acceptor through the H of the pyridinium, resulting in the formation of layers parallel to the (100) plane (Figure 2).

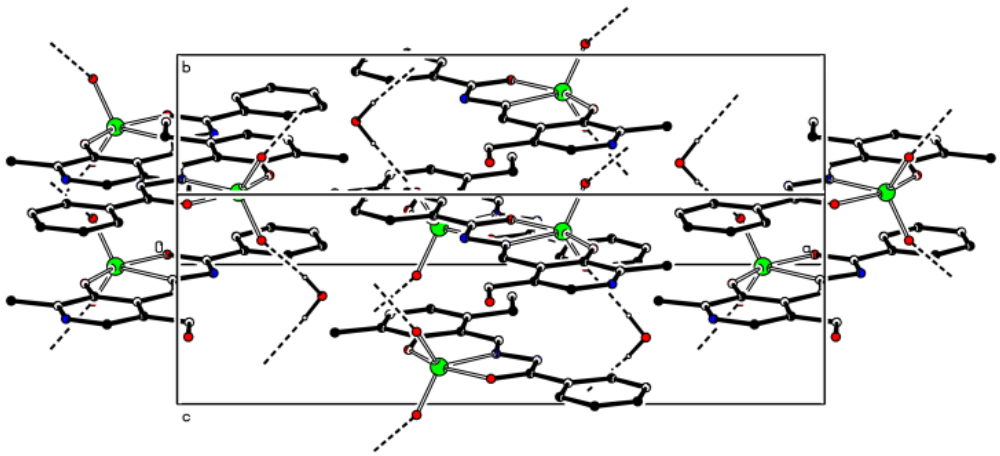

Figure 2. Packing of the complex **5** in the unit cell. Hydrogen bonds are shown by dotted lines between water molecules and vanadium complexes. The disordered methanol molecules were removed for clarity.

Within these layers, there are weak slipped π-π stacking interactions (centroid to centroid = 3.6128(6) Å and interplanar distance = 3.3320(1) Å with a slippage of 1.397 Å). These layers

are further interconnected through O–H···O hydrogen bonds involving the OH of the methanol solvate and the hydroxyl group attached to the complex (see Table 3), thus building a three dimensional network.

Table 3 Relevant hydrogen bonding parameters (distances in Å, angles in degrees) for the structure of compound **5.**

D—H···*A*	*D*—H	H···*A*	*D*···*A*	*D*—H···*A*
O16—H16···O21	0.82	1.87	2.691(3)	176
N3—H3···O5	0.86	1.87	2.733(3)	176
O21—H21···O16^{iii}	0.82	1.89	2.704(3)	169
O5—H5···O1^{iv}	0.85	1.99	2.825(2)	172

Symmetry codes: (iii) −*x*, −*y*+1, −*z* –x, -1/2+y, 2-z; (iv) −*x*+1/2, −*y*+1, *z*−1/2 -1/2-x, -y, ½+z

The structure of complex **5** is very close to the structure previously described for complex [$VO_2(H_2L^3)$] (**5***) [27] which crystallizes with a pyridine molecule and the structure is stabilized by *π*–*π* stacking. In addition to the different solvation (one molecule of pyridine for **5*** *vs.* one molecule of methanol and one of water for **5**), compound **5*** contains one additional H atom bonded to the N atom corresponding to atom N(2) in Figure 1, making it formally a complex of vanadium(IV). In that case, the metal coordination geometry is closer to square pyramidal with a value of the *τ* parameter [32] of 0.10, *vs.* 0.51 for **5** (an overlay of the two structures is shown in Figure 3). A comparison of the most significant parameters of the two experimental structures is presented in Table 4. It can be appreciated that all bond distances are nearly identical, including those to the two oxido ligands. The most striking difference can be seen in the N(1)–V–O(1) and N(1)–V–O(1i) angles, which are identical (imposed by the mirror symmetry) at 125.03(5)° in **5** and quite different in **5*** (107.17(9) and 142.60(10)°).

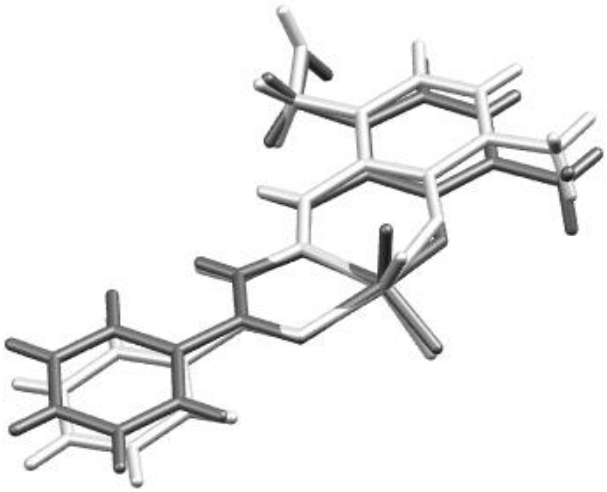

Figure 3. Overlay of the geometries of the complex **5** (dark grey) and **5*** (light grey).

Table 4. Comparison of relevant bond lengths (Å) between experimental data for **5** and **5*** and with the DFT optimized **V.**

Bonds	**5**	**V**	**5*** [a]
V–O(1)	1.619(1)	1.599	1.636(2)
V–O(1i)	1.619(1)	1.597	1.615(2)
V–O(12)	1.913(2)	1.956	1.937(2)
V–O(3)	1.950(2)	1.981	1.981(2)
V–N(1)	2.153(2)	2.285	2.147(2)
N(1)–N(2)	1.398(3)	1.342	1.378(3)
Angles			
O(1)–V–O(1i)	109.52(11)	110.83	109.69
O(1)–V–O(12)	97.93(6)	104.30	95.37
O(1)–V–O(3)	96.08(6)	105.75	93.66
O(12)–V–O(3)	155.58(9)	140.26	148.81
O(1)–V–N(1)	125.03(5)	101.22	107.17(9)
O(1i)–V–N(1)	125.03(5)	147.72	142.60(10)
O(12)–V–N(1)	82.02(8)	78.20	81.80
O(3)–V–N(1)	73.56(8)	70.92	73.05

[a] From reference 20. The labelling scheme follows that of compound **5**.

It is pertinent to remark that a search in the Cambridge structural database for mononuclear 5-coordinated complexes containing a VO_2 moiety yielded 160 hits of which only three are complexes of vanadium(IV). The other two compounds in addition to **5*** are $[VO_2(^{iPr}BPDI)]$ (^{iPr}BPDI = substituted bis(imino)pyridine) [33] and $[VO_2(H_2hasc)]$ (H_2hasc = 2-hydroxy-acetophenone-semicarbazone) [34]. For the former, an EPR study backed up by DFT calculations reveals that the spin density is mostly localized on the bis(imino)pyridine ligand,

thus the complex is in reality a vanadium(V) complex with a ^{iPr}BPDI ligand anion radical. The [VO_2(H_2hasc)] complex, on the other hand, appears to be a genuine vanadium(IV) species according to EPR spectroscopy and the structure of the related vanadium(V) complex [VO_2(Hhasc)] is also described in the same contribution. The comparison of these two structures is interesting in relation to our interest in **5** and **5*** because they are in both cases pairs of complexes with the same ligand, which is neutral in the vanadium(IV) complexes, [VO_2(H_2hasc)] and [VO_2(H_2L^3)] (**5***), while deprotonated in the vanadium(V) complexes, [VO_2(Hhasc)] and [VO_2(HL^3)] (**5**). The geometries of [VO_2(H_2hasc)] and [VO_2(Hhasc)] are very similar to each other and similar to that of **5***, namely close to a square pyramidal geometry. The N–V–O angles are 105.0(2) and 146.4(2)° in [VO_2(H_2hasc)] *vs.* 98.26(13) and 154.64(12)° in [VO_2(Hhasc)].[27] The τ parameter is 0.02 in [VO_2(H_2hasc)] and 0.16 in [VO_2(Hhasc)]. There is also no significant difference between the bond lengths for the bonds linking the vanadium to its donor atoms between the [VO_2(H_2hasc)] and [VO_2(Hhasc)] complexes, as found for the pair of complexes **5** and **5*** in Table 4. In conclusion, it seems that both vanadium(IV) and vanadium(V) prefer a square pyramidal geometry and that the bond distances are little sensitive to the oxidation state change. The adoption of an unusual more symmetric geometry by compound **5** could perhaps result from the hydrogen bonding network and the subsequent molecular packing imposed in the crystal.

3.4. DFT calculations on the structural issues

The DFT study was undertaken with the purpose of better understanding the structural difference between **5** and **5***. Starting from the geometry of the isolated molecule in the X-ray structure of **5** (excluding water and methanol), the structure converged to a geometry (**V**) (Figure 4), rather close to that already reported [27] for **5*** as can be evaluated in Table 3. This result appears to confirm the importance of the solvent molecules in the crystals for imposing the observed unusual geometry of **5**. It is relevant to mention that a related structure also showing a symmetric VO_2 moiety has been reported for a related [VO_2(LH)] complex with a similar *ONO* type Schiff base ligand, where the two symmetry-related N–V–O angles are 125.16(5)°. A solvent molecule, water in this case, is again part of the crystal habit [35].

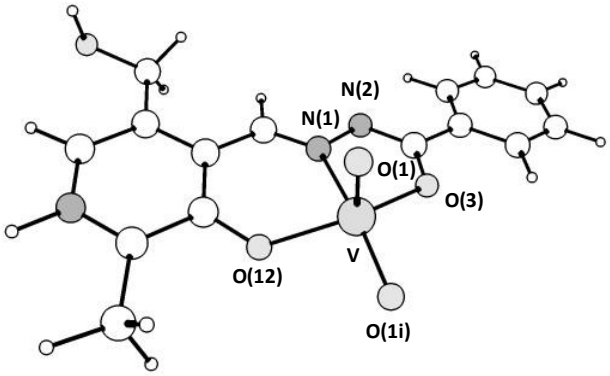

Figure 4. View of the optimized geometry of compound **5** (**V**).

Additional calculations were carried out starting from the experimental geometry of **5*** (yielding the optimized geometry **V***), and also after adding an H atom to the optimized **V**, yielding a new geometry **V**+H of formally vanadium(IV), and after removing one hydrogen from **V*** in order to obtain a new optimized geometry **V***-H of formally vanadium(V). The optimized geometries of compounds with the same formula (**V/V*-H** and **V*/V+H**) are very similar (Table 5). The V=O distances are essentially identical in both oxidation states, thus this criterion cannot be used to determine the oxidation state. The O–V–N bond angles deviate more from the ideal *tbp* values of 120° for the calculated V^{V} structures than for the calculated V^{IV} structures, in agreement with the experimental trend shown above for the complexes containing the hasc ligand. The trigonality index τ is greater for the V^{IV} geometries with values close to 0.20 whereas those of vanadium(V) yield values close to 0.10. In conclusion, the DFT calculation confirm the veracity of the structural determination of **5*** as a compound of vanadium(IV) and illustrates the little effect of the oxidation state, lower than that of crystal packing, on the structural parameters.

Table 5- Selected experimental (**5**, **5***) and theoretical (**V**, **V*-H**, **V***, **V+H**) angles, corresponding τ values and theoretical V-O vibrational values.

	5	**V**	**V*-H**	**5***	**V***	**V+H**
Distances						
V–O(1)	1.619(1)	1.599	1.598	1.636(2)	1.598	1.599
V–O(1i)	1.619(1)	1.597	1.598	1.615(2)	1.599	1.598
Angles						
O(1)–V–N(1)	125.03(5)	147.72	146.56	142.60(10)	136.16	137.03
O(1i)–V–N(1)	125.03(5)	101.22	102.35	107.17(9)	111.57	110.74
τ	0.51	0.12	0.09	0.10	0.20	0.18

3.5. Catalytic studies

All new complexes **1-7** have been tested as (pre)catalysts for the epoxidation of cyclooctene under solvent-free conditions, following a previously established procedure [8c, 17]. The oxido-bridged bis-vanadium complexes of general formula $[V_2O_3L_2]$ (**1-4**) are sparingly soluble in cyclooctene and insoluble in water at room temperature. However, they dissolve completely in the organic phase after addition of aqueous TBHP at 80 °C. The aqueous phase was colourless and the organic one orange-red, indicating that the catalyst is mainly confined in the organic phase. The epoxidation reaction was followed during five hours by withdrawing and analysing aliquots of the organic phase and the conversion results are shown in Figure 5. The cyclooctene conversion was moderate to very good after 5 h (60–87%), following the order **2** > **4** > **3** > **1**. In all cases, but more markedly for complex **3**, the activity is initially high but decreases after the first half hour, showing either conversion of an initially active catalyst into a less active form, or catalyst inhibition by the reaction product.

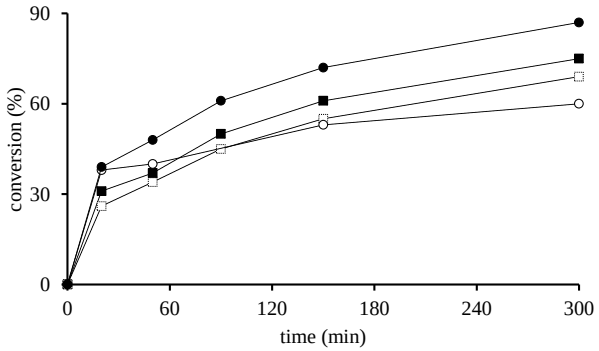

Figure 5. Kinetic profile of converted cyclooctene *vs.* time with oxido-bridged bis-vanadium(V) (pre)catalysts: complex **1** (○)**,** complex **2** (●), complex **3** (□), complex **4** (■). Conditions: substrate/complex = 2000:1; T = 80 °C.

The mononuclear dioxidovanadium(V) complexes **5-7** did not completely dissolve in the organic phase after addition of aqueous TBHP at 80 °C and a yellow-orange precipitate (characterized by IR and ^{51}V NMR as the unsolvated molecule in the case of **6**) was formed as the reaction progressed. The epoxidation results are shown in Figure 6. The observed cyclooctene conversion was lower than in the presence of the oxido-bridged bis-vanadium(V) complexes under the same conditions, (26-33%) following the order **6** > **7** > **5**. The initial catalytic activity is high also with these pre-catalysts, comparable with that of **1-4**, but the deactivation or inhibition effect seems to be stronger. The change in conversion slope may be related to precipitation of the unsolvated complex, hence decreasing the effective catalyst concentration in solution.

The selectivity towards the formation of cyclooctene oxide for all tested compounds is low (Table6). The major product is the corresponding cyclooctanediol, as qualitatively observed in the chromatograms. However, this product could not be quantified because part of it remains in the aqueous phase. Considering the low catalyst loading (0.05 % [V] *vs*. substrate), the initial turnover frequencies (TOF_{20min}, reported in Table 6) are quite good, from 940 h^{-1} for complex **5** up to 2339 h^{-1} for complex **1**. Under these conditions, the [$VO(acac)_2$] compound gives a TOF of 1354 h^{-1} and a higher selectivity but could not be recovered. The H_2L ligands alone were not active at all. The TOF values were higher for the *ONS* based compounds **1**–**4**.

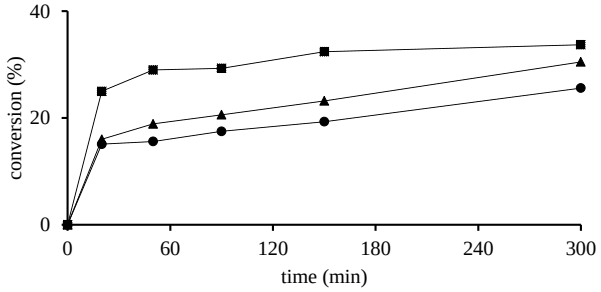

Figure 6. Kinetic profile of converted cyclooctene *vs.* time with dioxidovanadium(V) (pre)catalysts: complex **5** (●), complex **6** (■), complex **7** (▲),Conditions: substrate/complex = 2000:1; T = 80 °C.

Table 6. Relative data of epoxidation catalysis toward cyclooctene.

Complex	**1**	**2**	**3**	**4**	**5**	**6**	**7**	**[$VO(acac)_2$]**
Conversion[a] (%)	61	87	67	74	26	33	31	75
Selectivity[b] (%)	35	32	30	36	10	10	13	87
TOF_{20min}[c] (h^{-1})	2339	2409	1587	1930	940	1571	1179	1354
TON[d]	1251	1804	1386	1551	532	700	633	1500

[a] Calculated after 5 h. [b] formed epoxide per converted olefin after 5 h. [c] cyclooctene transformed / catalyst / time at 20 minutes [d] cyclooctene transformed / catalyst at 5 h.

As mentioned above, the epoxidation processes run with the dioxidovanadium(V) (pre)catalysts **5**–**7** gave rise to the formation of a yellow-orange precipitate. Since **6** yielded the largest amount of precipitate (ca. half of the initial mass), this precipitate was used for a second run (**6***) (procedure B), and the precipitate resulting from this new experiment (**6****, one quarter of initial mass of **6**) for a third run (procedure C). For each run, the amounts of starting cyclooctene and TBHP were kept constant. A fourth run was also carried out with a fivefold amount (0.25% relative to substrate) of fresh pre-catalyst **6**. The kinetic profiles for each run are shown in Figure 7and the essential data are summarized in Table 6. While the

final conversion after 5 h and the selectivity differ somewhat, the kinetic profile of the four runs is essentially the same, with an initial period of high activity followed by a longer period of much lower activity. This behaviour is consistent with a product inhibition phenomenon (maybe due to the interaction with the formed products) or to the complex precipitation and not with catalyst deactivation. The relative independence of the kinetic profile on the catalyst amount (0.05% vs. 0.25 %), given that this (pre)catalyst does not completely dissolve in the reaction medium, shows that the activity is limited by the solubility. Therefore, it is not necessary to use large catalyst loadings. Finally, the activity of the recycled catalysts (**6*** and **6****) is essentially identical to that of **6**, suggesting the absence of catalyst degradation. However, an IR study of the catalytic species **6** and **6*** in the *ν*(V=O) region does not reveal important changes (Figure 8). This suggests that the chemical or at least structural nature of the catalyst remains constant during the catalytic runs, without affecting the catalyst performance. No signals corresponding to a peroxo intermediate [19] could be detected in the IR spectrum as well as in ^{51}V NMR for the recovered catalyst **6***.

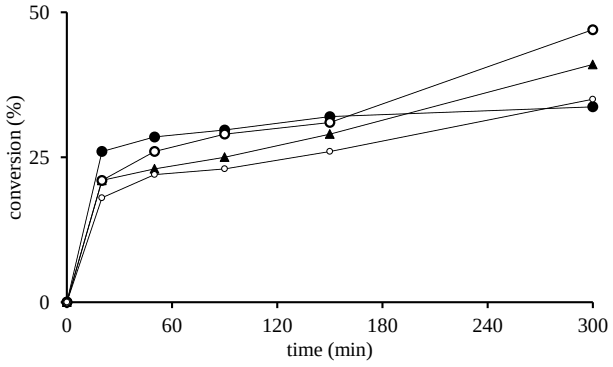

Figure 7. Kinetic profile of converted cyclooctene *vs.* time with (pre)catalysts 6: --●-- 0.05% [V] complex 6, --○-- complex 6*, --○-- complex 6**, --▲--0.25% [V] complex . Conditions: T = 80 °C.

Table 6 Relative data of epoxidation catalysis toward cyclooctene.

Complex	0.05% [**6**]	**6***	**6****	0.25% [**6**]
Conversion[a] (%)	34	47	35	41
Selectivity[b] (%)	10	24	10	12
TOF_{20min}[c] (h^{-1})	1571	-	-	265
TON[d]	700	-	-	170

[a] After 5 h. [b] Formed epoxide per converted olefin after 5 h. [c] Cyclooctene transformed / catalyst / time at 20 minutes. [d] Cyclooctene transformed / catalyst at 5 h.
* First recycle of used catalyst. ** Second recycle of used catalyst.

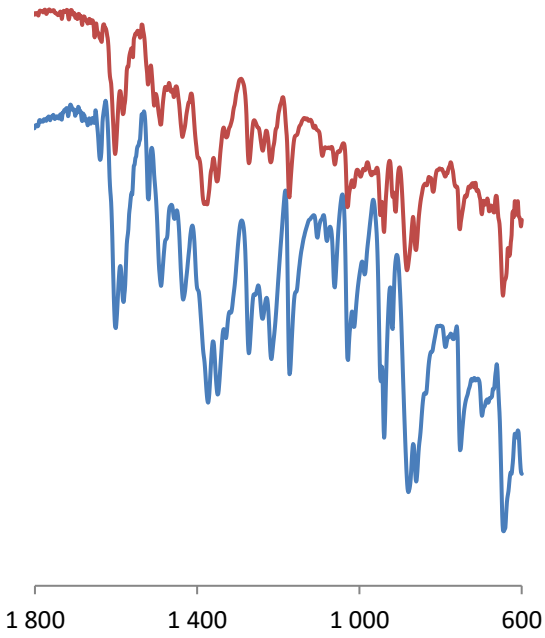

Figure 8. Comparison of the IR vibrations of the catalytic materials **6**(blue), **6***(red) in the V=O stretching region.

3.6. DFT studies of the catalytic mechanism

The mechanism of catalytic epoxidation has been the subject of keen interest and debate for decades, since the contrasting propositions by Mimoun [36] and Sharpless [37] (vide infra). It is inappropriate to summarize the state of the art here, except for pointing out that computational studies involving vanadium catalysts are very limited [38] and deal with H_2O_2 as the oxidizing agent with only one exception [38e]. When H_2O_2 is the oxidant, proton exchange processes allow the facile formation of peroxido ligands with water elimination and the key oxygen atom transfer step can then proceed from the V(OO) moiety to the olefin substrate. Besides the Mimoun and the Sharpless pathways, a third pathway involving a vanadium(IV) peroxido radical species has also been invoked in experimental studies based on $VO(acac)_2$ [39] and on vanadium-substituted phosphomolybdic acid [40] catalysts. The theoretical studies carried out so far are in favour of the classical Sharpless mechanism, which is represented in Scheme 3 (left). However, when the oxidant is TBHP, regeneration of the peroxido ligand from a V=O function and TBHP through intermediate **B** (R = *t*Bu) is not expected to be facile.

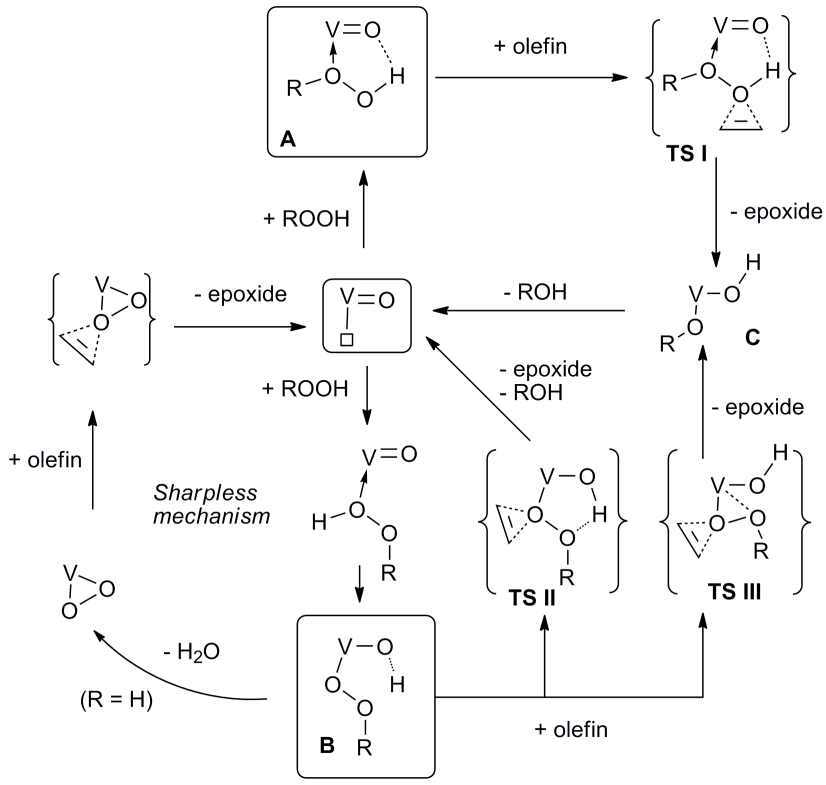

Scheme 3. Possible mechanistic pathways for olefin epoxidation by vanadium catalyst.

Possible ways to go around this problem involve direct transfer to the olefin of an O atom from the TBHP molecule which is either coordinated to the metal center, V(O)(*t*BuOOH), as in intermediate **A** of Scheme 3leading to **TS I**, or activated by proton transfer to the oxido ligand and generation of an alkylperoxido intermediate, V(OO*t*Bu)(OH), as in intermediate **B** which leads to **TS II** or **TS III**. While **TS II** involves assistance by an H-bond between the OH ligand as a proton donor and the OOR ligand as a proton acceptor, **TS III** involves assistance by an incipient interaction between the metal atom and the O^{β} atom (we use a nomenclature where atom O^{α} binds the H atom in TBHP or the V atom in the *tert*-butylperoxido complex, whereas atom O^{β} is the atom bearing the *t*Bu group: V-O^{α}-O^{β}-*t*Bu, H-O^{α}-O^{β}-*t*Bu). Note that the pathway via **TS II** leads to a concerted and direct generation of both products (epoxide and ROH), whereas the other two pathways lead to an alkoxido-hydroxydo intermediate **C** via elimination of the epoxide, whereas the ROH by-product must be formed in a subsequent step. All these alternatives still involve, however, direct O-atom transfer to the olefin substrate as in the Sharpless mechanism, rather than via olefin coordination and insertion as in the Mimoun mechanism.

These variants of the Sharpless mechanism have so far been examined computationally for few catalytic systems (Ti,[41] Mo,[16, 42] W[43]), but not for vanadium. However, a

pathway of this kind (through a transition state similar to **TS III**) was computationally found as the preferred one for the oxygen transfer from H_2O_2 to R_2S_2 catalysed by a Schiff base complex of V^V, in spite of the potential access in this case to the peroxido intermediate for a classical Sharpless-type mechanism [44]. Formation of intermediate **A**, which is stabilized by a H-bond to an oxido ligand, requires an open coordination site on the metal centre, as found for instance in 5-coordinate complexes of type $[MoO_2(L)]$ (L = tridentate dianionic ligand) [16a]. The evolution of **B** via a transition state of type **TS II**, which is stabilized by the H-bond in the 5-membered cycle, was shows to be the preferred pathway for a 6-coordinate complex of type type $[MoO_2(L)]$ (L = tetradentate dianionic ligand) [42a], whereas all the calculations on the Ti catalysts [41] and on the organometallic $[Cp^*WO_2Cl]$ systems [42d,43a] highlight a pathway through a transition state of type **TS III**.

For both structural types investigated here, namely dinuclear $[V_2O_3L_2]$ and mononuclear $[VO_2(LH)]$, all pathways involving **TS I**, **TS II** or **TS III** as transition states are possible in principle. Indeed, a 5-coordinated vanadium centre is present for coordinative addition of TBHP and a V=O function is available for activation by proton transfer. Both types of complexes are moderately active towards epoxidation. The same active species is in principle accessible from both types of catalysts, because $[V_2O_3L_2]$ can equilibrate with mononuclear [VO(OH)L] in the presence of water, and the latter is a tautomeric form of $[VO_2(LH)]$. Alkoxido oxido complexes [LVO(OR)] have been isolated previously with other type of ONS ligands and different alkoxido groups [45]. Therefore, we have explored the three possible pathways using only the complex with the ONO-type pyridoxal benzhydrazido ligand that was structurally characterized in this contribution.

Our calculations have addressed a simplified model of the mononuclear $[VO_2(HL)]$ complex where the pending methyl and hydroxymethyl substituents were replaced by hydrogen atoms, *t*BuOOH was modelled by MeOOH and the olefin substrate was modelled by ethylene, in order to save computational time. The calculations were carried out in the gas phase. We did not consider it necessary to carry out a solvation correction. The oxidant was introduced as an aqueous solution, but water is not miscible with the substrate whereas *t*BuOOH migrates to the organic phase where the catalyst is also located. The solvent medium is therefore essentially a mixture of olefin and *t*BuOOH (which later transforms into *t*BuOH) and the polarity is difficult to estimate but is considered as sufficiently low and should not affect significantly the energies that are estimated in the gas phase.

A pathway involving intermediate **A** of Scheme 3could not be located, because every attempt to optimize the geometry of this adduct as represented in Scheme 3 led to expulsion

of the alkyl hydroperoxide. This result is in stark contrast with the 5-coordinate Mo analogue [MoO_2(L)], which yields a stable 6-coordinate local minimum for the adduct [MoO_2(L)(TBHP)] and correlates with the lower propensity of 5-coordinate VO_2^+ derivatives to increase their coordination number. The calculation led to an H-bonded adduct, [VO(HL)(=O···HOOMe)], featuring a strong H-bond between MeOOH as a proton donor and one of the oxido ligands of **V** as a proton acceptor (O···H distance of 1.757 Å), which is stabilized by 20.8 kcal/mol on the electronic energy scale (9.9 kcal/mol in free energy) relative to the two separate adducts. The strength of this H-bonding interaction reflects the electron donor power and polarity of the V=O function and the strong proton donating ability of the hydroperoxide. This is the most stable species and is therefore the resting state (or rate-determining intermediate) of the catalytic cycle.

For the [VO(OH)(OOMe)(HL)] stoichiometry (intermediate **B** of Scheme 3), two different local minima could be optimized, one with a H-bond between the OH proton and the OOMe O^β atom (at –10.3 kcal/mol relative to the separate reagents, **B2**) and one without (at –5.6 kcal/mol, **B1**), see Figure 9. Note that both local minima are at higher energy than the precursor MeOOH adduct, thus proton transfer with activation of the MeOOH reagent is endothermic. Using the geometry of **B1** as a starting point, a transition state **TS III** could be located at 26.4 kcal/mol. In this transition state, the O^α–O^β bond is significantly elongated relative to the **B1** intermediate (from 1.428 to 1.827 Å) whereas the V–O^α remains rather short (changing from 1.938 to 1.994 Å) while the two olefin C atoms have significantly approached the O^α atom (1.963 and 2.107 Å), the olefin C=C bond is slightly elongated to 1.365 Å and the V and O^β atoms have already established a significant interaction (2.050 Å). Epoxide elimination is very exothermic and leads to the [VO(OH)(OMe)(HL)] intermediate located at –46.1 kcal/mol, which then rearranges to the starting dioxido catalyst with a MeOH molecule H-bonded to one of the two O ligands, [VO(HL)(=O···HOMe)], with a further thermodynamic gain. The cycle is closed by replacement of the H-bonded MeOH molecule by a new molecule of the MeOOH oxidant with a further energy gain of 1.9 kcal/mol. The energy span of this cycle is very high (47.2 kcal/mol from the rate-determining intermediate **A** to the rate-determining transition state **TS III**). On the other hand, starting from the H-bonded minimum **B2**, a transition state **TS II** in Scheme 3was found at a relative energy of 10.5 kcal/mol, see Figure 9. In this transition state, both the V–O^α and the O^α–O^β bonds are significantly elongated relative to the [VO(OH)(OOMe)(HL)] intermediate **B2** (from 2.079 to 3.160 Å for the former, from 1.458 to 1.709 Å for the latter), while the O^α atom establishes incipient interactions with the olefin C atoms (2.141 and 2.252 Å), the olefin C=C double

bond is slightly elongated (1.348 Å), the V–OH proton is already closer to the O^{β} atom of the former –OOMe ligand than to the OH oxygen atom, and the V–O distance to the former OH ligand has considerably shortened (from 1.702 to 1.015 Å). All these parameters indicate the "late" nature of the transition state, as expected for a very exothermic process. Indeed, the TS leads directly to the free epoxide and to a H-bonded MeOH adduct, [VO(HL)(=O···HOMe)] The energy span of this cycle is 31.3 kcal/mol, much lower than that of the other cycle examined above.

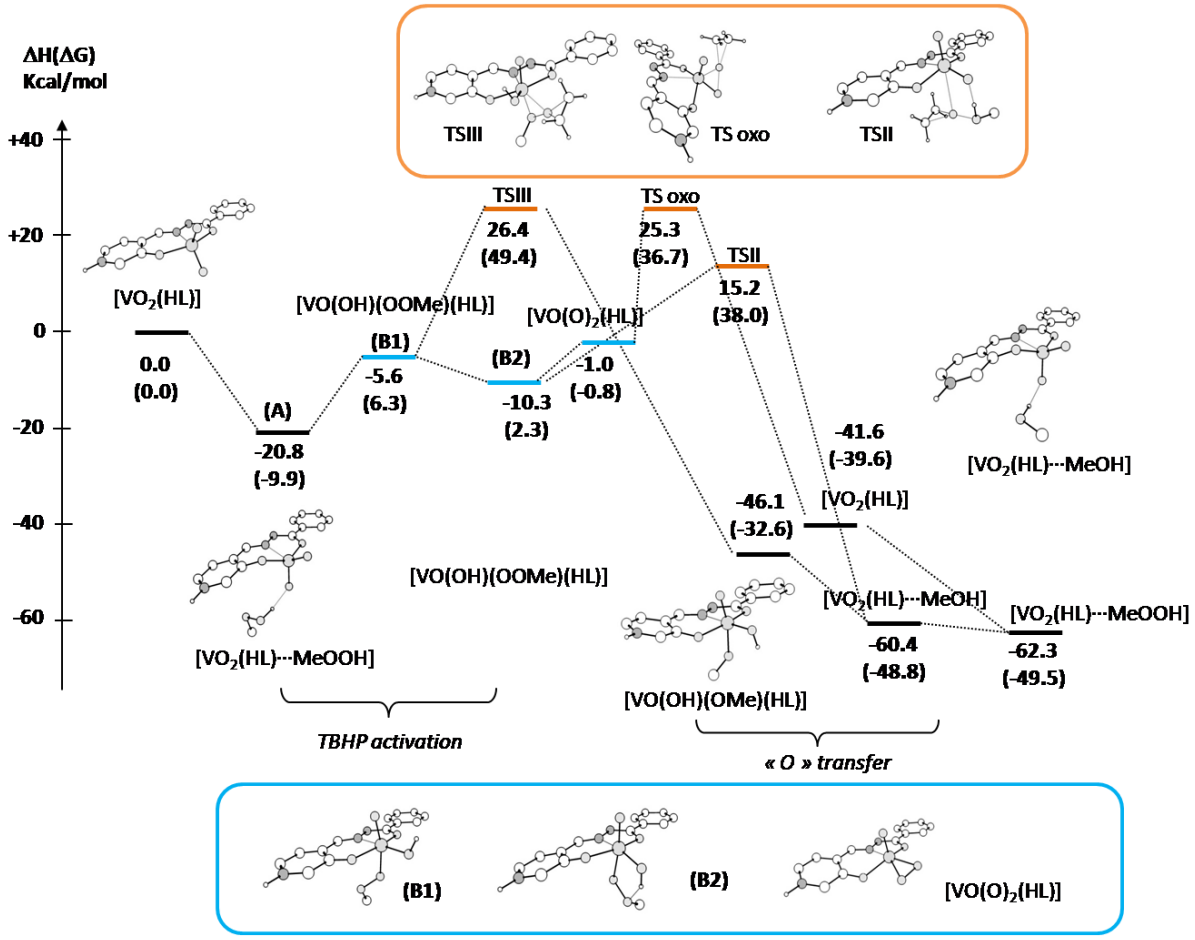

Figure 9. Energy diagram of the epoxidation of ethylene by MeOOH catalyzed by $[VO_2(HL)]$ and views of the optimized structures (non relevant hydrogen atoms were removed for clarity).

The structure of compound $[VO(O_2)(HL)]$, which may be generated from intermediate **B2** by MeOH elimination, was also optimized. It is located at –1.1 kcal/mol on the E scale of Figure 9 (–0.8 kcal/mol on the G scale). However, as previously discussed, its formation from **B2** is expected to be associated to a high energy barrier, which was not calculated. Note that this intermediate is endothermic relative to **A**, therefore it is not expected to accumulate in the catalytic reaction, in agreement with the lack of experimental observation of peroxide species. Assuming that this intermediate would anyhow be kinetically accessible during catalysis, it

could in principle transfer an O atom to the olefin by one of the classical Sharpless or Mimoun mechanisms. Therefore, the TS of the O atom transfer from [$VO(O_2)(HL)$] to ethylene has also been calculated (**TS oxo,** Figure 9). The energy of **TS oxo** is higher than that of **TS II** by ca. 10 Kcal/mol (H scale) and close to that of **TS III**. Therefore, the calculations do not support the involvement of peroxide species in epoxidation catalyzed by this type of vanadium system.

The energy span of the best calculated cycle from the resting state **A** to the rate-determining transition state **TS II** is 31.3 kcal/mol on the E scale (47.9 kcal/mol on the G scale). The high value of the activation free energy is justified by its strongly associative nature and is certainly overestimated given the full consideration of the translational and rotational degrees of freedom in the gas phase calculation, whereas these are extensively quenched in the condensed phase. The energy span of this cycle is not unreasonable given the observed catalytic activity. A lower energy span of 22.5 kcal/mol was calculated for the [MoO_2(SAP)] system, which indeed displays a considerably greater catalytic activity [16a]. In summary, the calculations have located a viable pathway for the activation of the hydroperoxide oxidant and O atom transfer to olefin, which involves proton transfer and H-bonded assisted O atom transfer to external olefin from a hydroxido-alkylperoxido intermediate.

4. Conclusions

New V^V complexes with Schiff bases derived from pyridoxal and pyridoxal hydrochloride were synthesised. The crystal structure of complex **5** has been determined, confirming the tridentate *ONO* bonding of the ligand to the vanadium atom, as well as protonation of the pyridine ring. The structure is very similar to that of a V(IV) derivative with a neutral ligand, [$VO_2(H_2L^3)$], except for an unusual trigonal bipyramidal geometry, which has been attributed to crystal packing effects. All vanadium complexes have been used as (pre)catalysts at 0.05% loading for epoxidation reactions of *cis*-cyclooctene under "green" reaction conditions, namely using aqueous TBHP as oxidising agent and without using any extra solvent. The dinuclear oxido-vanadium(V) complexes have shown the best catalytic activity and selectivity among all tested compounds. Different mechanistic possibilities for the catalyzed O atom transfer to olefin have been addressed by the DFT calculation. Two of the explored pathways were shown to be viable, with one of them having a lower energy span. It corresponds to the H-bond assisted transfer of the O^{α} to an external olefin, a pathway that has been investigated

before for Mo^{VI} systems but never explored for V^{V}. In addition, the calculations do not support the involvement of peroxido complexes as kinetically viable catalytic intermediates.

5. Acknowledgments

All authors acknowledge the CNRS, the University Paul Sabatier (Institut Universitaire Paul Sabatier) and the Institut Universitaire de France for all research facilities and for funding. The fellowship of Jana Pisk was provided by Ministry of Science, Education and Sports of the Republic of Croatia and by the French Embassy in Croatia. This work was granted access to the HPC resources of CINES under the allocation 2013-086343 made by GENCI (Grand Equipement National de Calcul Intensif) and to the resources of the CICT (Centre Interuniversitaire de Calcul de Toulouse, project CALMIP). Weili Wang is acknowledged for technical assistance. Christian Bijani from LCC is acknowledged for the ^{51}V NMR measurements.

Supporting Information

Cartesian coordinates and drawings for all calculated structures (4 pages).

Notes and references

[1] (a) D. Rehder, Inorg. Chem. Commun. 6 (2003) 604-617. (b) P. S. Maia, V. M. Deflon, E. J. Souza, E. Garcia, A. A. Batista, A. T. Figueiredo, E. Niquet, Trans. Met. Chem. 30 (2005) 404–410. (c) M. R. Maurya, A. Arya, A. Kumar, J. C. Pessoa, Dalton Trans. 12 (2009) 2185–2195. (d) K. C. Bolm, Coord. Chem. Rev. 237 (2003) 245–256. (e) S. Gambarotta, Coord. Chem. Rev. 237 (2003) 229–243. (f) A. G. J. Ligtenbarg, R. Hage, B. L. Feringa, Coord. Chem. Rev. 237 (2003) 89–101. (f) D. Wischang, O. Brücher, J. Hartung, Coord. Chem. Rev. 255 (2011) 2204–2217. (g) M. R. Maurya, S. Khurana, Shailendra, A. Azam, W. Zhang, D. Rehder, Eur. J. Inorg. Chem., (2003) 1966-1973. (h) P. Noblıa, E. J. Baran, L. Otero, P. Draper, H. Cerecetto, M. González, O. E. Piro, E. E. Castellano, T. Inohara,Y. Adachi, H. Sakurai, D. Gambino, Eur. J. Inorg. Chem., (2004) 322–328. (i) S. Takizawa, F. Arteaga Arteaga, Y. Yoshida, J. Kodera, Y. Nagata, H. Sasai, Dalton Trans. 42 (2013) 11787-11790. (j) A. A. Holder, P. Taylor, A. R. Magnusen, E. T. Moffett, K. Meyer, Y. Hong, S. E. Ramsdale, M. Gordon, J. Stubbs, L. A. Seymour, D. Acharya, R. T. Weber, P. F. Smith, G. C. Dismukes, P. Ji, L. Menocal, F. Bai, J. L. Williams, D. M. Cropek, W. L. Jarrett, Dalton Trans. 42 (2013) 11881-11899. (k) M. Fernández, J. Varela, I. Correia, E. Birriel, J. Castiglioni, V. Moreno, J. C. Pessoa, H. Cerecetto, M. González, D.

Gambino, Dalton Trans. 42 (2013) 11900-11911. (l) M. R. Maurya, C. Haldar, A. Kumar, M. L. Kuznetsov, F. Avecilla, J. C. Pessoa, Dalton Trans. 42 (2013) 11941-11962. (m) M. Sutradhar, N. V. Shvydkiy, M. F. C. Guedes da Silva, M. V. Kirillova, Y. N. Kozlov, A. J. L. Pombeiro, G. B. Shul'pin, Dalton Trans. 42 (2013) 11791-11803. (n) G. Licini, V. Conte, A. Coletti, M. Mba, C. Zonta, Coord. Chem. Rev. 255 (2011) 2345-2357.

[2] (a) D. Rehder, Bioinorganic Vanadium Chemistry, Wiley-WCH, Weinheim (2008) 13-26. (b) A. S. Tracey, G. R. Willsky, E. S. Takeuchi, Vanadium: Chemistry, Biochemistry, Pharmacology and Practical Applications, CRC Press, Boca Raton (2007) 181-185.

[3] P. B. Chatterjee, K. Bhattacharya, M. Chaudhury, Coord. Chem. Rev. 255 (2011) 2150–2164.

[4] S. Floquet, M. C. Muñoz, R. Guillot, E. Rivière, G. Blain, J. A. Réal, M. L. Boillot, Inorg. Chim. Acta, 362 (2009) 56-64.

[5] (a) A. E. Martell, Metal Ions in Biological Systems, ed. H. Sygel , Dekker, New York, 2 (1973) 207-268. (b) J. T. Cutfield, D. Hall, T. N. Walters, Chem. Commun. (1967) 785–786. (c) F. Nepveu, J. J. Bonnet, J. P. Laurent, J. Coord. Chem. 11 (1981) 185–193.

[6] (a) A. Butler, M. J. Clague, G. E. Meister, Chem. Rev. 94 (1994) 625–638. (b) M. R. Maurya, Coord. Chem. Rev. 237 (2003) 163–181. (c) K. A. Jorgensen, Chem. Rev. 89 (1989) 431-485. (d) J. Hartung, S. Drees, M. Greb, P. Schmidt, I. Svoboda, H. Fuess, A. Murso, D. Stalke, Eur. J. Org. Chem. (2003) 2388-2408. (e) M. Greb, J. Hartung, F. Köhler, K. Spehar, R. Kluge, R. Csuk, Eur. J. Org. Chem. (2004) 3799-3812. (f) J. Hartung, Pure Appl.Chem. 77 (2005) 1559–1574. (g) S. Bellemin-Laponnaz, K. S. Coleman, P. Dierkes, J.-P. Masson, J. A. Osborn, Eur. J. Inorg. Chem. (2000) 1645-1649. (h) R. A. Shiels, K. Venkatasubbaiah, C. W. Jones, Adv. Synth. Catal., 350 (2008) 2823–2834. (i) M. R. Maurya, A. A. Khan, A. Azam, A. Kumar, S. Ranjan, N. Mondal, J. C. Pessoa, Eur. J. Inorg. Chem. (2009) 5377–5390.

[7] (a) Y. Wang, M. Wang, Y. Wang, X. Wang, L. Wang, L. Sun, J. Catal. 273 (2010) 177–181. (b) G. Romanowski, M. Wera, Polyhedron 29 (2010) 2747-2759. (c) J. Rahchamani, M. Behzad, A. Bezaatpour, V. Jahed, G. Dutkiewicz, M. Kubicki, M. Salehi, Polyhedron 30 (2011) 2611–2618. (d) P. Plitt, H. Pritzkow, R. Krämer, Dalton Trans. (2004) 2314–2320. (e) G. Romanowski, E. Kwiatkowski, W. Nowicki, M. Kwiatkowski, T. Lis, Polyhedron 27 (2008) 1601–1609. (f) E. Kwiatkowski, G. Romanowski, W. Nowicki, M. Kwiatkowski, K. Suwinska, Polyhedron 26 (2007) 2559–2568. (g) D. Balcells, F. Maseras, G. Ujaque, J. Am. Chem. Soc. 127 (2005) 3624-3634. (h) E. Kwiatkowski, G. Romanowski, W. Nowicki, M. Kwiatkowski, K. Suwinska, Polyhedron 22 (2003) 1009-1018. (i) G. Romanowski, J. Kira, Polyhedron 53 (2013) 172-178. (j) G. Romanowski, J. Mol. Catal. A: Chem. 368-369 (2013) 137-144. (k) G. Romanowski, M. Wera, Polyhedron 50 (2013) 179-186. (l) G. Romanowski, T. Lis, Inorg. Chim. Acta 394 (2013) 627-634.

[8] (a) V. Conte, B. Floris , Dalton Trans. 40 (2011) 1419–1436. (b) N. L. Silva, C. B. Pinheiro, E. P. Chacon, J. A. L. C. Resende, J. W. de M. Carneiro, T. L. Fernández, M. Scarpellini, M. Lanzaster, J. Braz. Chem. Soc. 22 (2011) 660–668. (c) C. Cordelle, D. Agustin, J. C. Daran, R. Poli, Inorg. Chim. Acta 364 (2010) 144–149. (d) H. H. Monfared, R. Bikas, P. Mayer, Inorg. Chim. Acta 363 (2010) 2574–2583. (e) M. R. Maurya, M. Bisht, A. Kumar, M. L. Kuznetsov, F. Avecilla, J. Costa Pessoa, Dalton Trans. 40 (2011) 6968-6983. (f) S. Rayati, N. Sadeghzadeh, H. R. Khavasi, Inorg. Chem. Commun. 10 (2007) 1545–1548. (g) M. R. Maurya, M. Bisht, F. Avecilla, J. Mol. Catal. A: Chem. 344 (2011) 18–27. (h) H. Hosseini-Monfared, R. Bikas, P. Mahboubi-Anarjan, S. W. Ng, E. R. T. Tiekink, Z. Anorg. Allg. Chem. 640 (2014) 243-248. (i) H. Hosseini-Monfared, A. Farrokhi, S. Alavi, P. Mayer, Trans. Met. Chem. 38 (2013) 267-273. (j) H. Hosseini Monfared, V. Abbasi, A. Rezaei, M. Ghorbanloo, A. Aghaei, Trans. Met. Chem. 37 (2012) 85-92. (k) M. Trivedi, R. Nagarajan, A. Kumar, N. P. Rath, J. Organomet. Chem. 695 (2010) 1722-1728. (l) Z. Li, H. Yamamoto, Acc. Chem. Res. 46 (2013) 506-518. (m) F. Madeira, S. Barroso, S. Namorado, P. M. Reis, B. Royo, A. M. Martins, Inorg. Chim. Acta 383 (2012) 152-156. (n) Y. Hoshino, H. Yamamoto, J. Am. Chem. Soc. 122 (2000) 10452-10453. (o) W. Zhang, A. Basak, Y. Kosugi, Y. Hoshino, H. Yamamoto, Angew. Chem., Int. Ed. 44 (2005) 4389-4391. (p) P. Adao, J. Costa Pessoa, R. T. Henriques, M. L. Kuznetsov, F. Avecilla, M. R. Maurya, U. Kumar, I. Correia, Inorg. Chem. 48 (2009) 3542-3561. (q) M. R. Maurya, S. Agarwal, M. Abid, A. Azam, C. Bader, M. Ebel, D. Rehder, Dalton Trans. (2006) 937-947. (r) K. I. Smith, L. L. Borer, M. M. Olmstead, Inorg. Chem. 42 (2003) 7410-7415.

[9] (a) Ed. E. N. Jacobsen, A. Pfaltz, H. Yamamoto, Comprehensive Asymmetric Catalysis, Springer-Verlag, Berlin (1999) 1178-1180. (b) I. M. Pastor, M. Yus, Curr. Org. Chem. 9 (2005) 1-29.

[10] H. U. Blaser, M. Studer, Green Chem. 5 (2003) 112-117.

[11) S. Liu, J. Xiao, J. Mol. Catal. A: Chem. 270 (2007) 1–43.

[12] (a) P. T. Anastas, J. C. Warner in Green Chemistry: Theory and Practice, ed. P. T. Anastas, T. C. Williamson, Oxford Science Publications, New York (1998) 1-26. (c) C. Li, T. Chen, Organic Reactions in Aqueous Media, Wiley Interscience, New York (1997). (d) C.-H. Li, W.-C. Zhang, J. Am. Chem. Soc., 120 (1998) 9102–9103.

[13] J. A. Gladysz, Recoverable and Recyclable Catalysts, ed. M. Benaglia, Wiley-WCH, Weinheim, (2009) 1-14.

[14] L. Gharnati, O. Walter, U. Arnold, M. Döring, Eur. J. Inorg. Chem. (2011) 2756–2762.

[15] B. Guérin, D. Mesquita Fernandes, J. -C. Daran, D. Agustin, R. Poli, New. J. Chem. 37 (2013) 3466-3475.

[16] (a) J. Morlot, N. Uyttebroeck, D. Agustin, R. Poli, ChemCatChem. 5 (2013) 601-611. (b) M. Loubidi, D. Agustin, A. Benharref, R. Poli, C. R. Chim. 17 (2014) 549–556. (c) W. Wang, T. Vanderbeeken, D. Agustin, R. Poli, Catal. Commun. (2014) DOI: 10.1016/j.catcom.2014.08.018

[17] (a) J. Pisk, D. Agustin, J. C. Daran, V. Vrdoljak, R. Poli, Adv. Synth. Catal. 353 (2011) 2910-2914. (b) J. Pisk, B. Prugovečki, D. Matković-Čalogović, R. Poli, D. Agustin, V. Vrdoljak, Polyhedron 33 (2012) 441-449. (c) J. Pisk, B. Prugovečki, D. Matković-Čalogović, T. Jednačak, P. Novak, D. Agustin, V. Vrdoljak, RSC Adv. 4 (2014) 39000-39010. (d) V. Vrdoljak, J. Pisk, D. Agustin, P. Novak, J. Parlov Vuković, D. Matković-Čalogović, New J. Chem. 38 (2014) 6176-6185.

[18] M. R. Maurya, S. Agarwal, C. Bader, D. Rehder, Eur. J. Inorg. Chem. (2005) 147-157.

[19] M. Ferrari Bellichi, F. Bisceglie, E. Leporati, G. Pelosi, P. Tarasconi, Bull. Chem. Soc. Jpn. 75 (2002) 781–788.

[20] M. J. Frisch, G. W. Trucks, H. B. Schlegel, G. E. Scuseria, M. A. Robb, J. R. Cheeseman, J. A. Montgomery Jr., T. Vreven, K. N. Kudin, J. C. Burant, J. M.Millam, S. S. Iyengar, J. Tomasi, V. Barone, B. Mennucci, M. Cossi, G. Scalmani, N. Rega, G. A. Petersson, H. Nakatsuji, M. Hada, M. Ehara, K.Toyota, R. Fukuda, J. Hasegawa, M. Ishida, T. Nakajima, Y. Honda, O. Kitao, H. Nakai, M. Klene, X. Li, J. E. Knox, H. P. Hratchian, J. B. Cross, V. Bakken, C. Adamo, J. Jaramillo, R. Gomperts, R. E. Stratmann, O. Yazyev, A. J. Austin, R. Cammi, C. Pomelli, J. W. Ochterski, P. Y. Ayala, K. Morokuma, G. A. Voth, P. Salvador, J. J. Dannenberg, V. G. Zakrzewski, S. Dapprich, A. D. Daniels, M. C. Strain, O. Farkas, D. K. Malick, A. D. Rabuck, K. Raghavachari, J. B. Foresman, J. V. Ortiz, Q. Cui, A. G. Baboul, S. Clifford, J. Cioslowski, B. B. Stefanov, G. Liu, A. Liashenko, P. Piskorz, I. Komaromi, R. L. Martin, D. J. Fox, T. Keith, M. A. Al-Laham, C. Y. Peng, A. Nanayakkara, M. Challacombe, P. M. W. Gill, B. Johnson,W. Chen, M. W. Wong, C. Gonzalez, J. A. Pople, GAUSSIAN 03, Revision D.01, Gaussian, Inc., Wallingford, CT, (2004).

[21] (a) A. D. Becke, J. Chem. Phys. 98 (1993) 5648–5625. (b) C. Lee, W. Yang, R. G. Parr, Phys. Rev. B 37 (1988) 785–789. (c) B. Miehlich, A. Savin, H. Stoll, H. Preuss, Chem. Phys. Lett. 157 (1989) 200–206.

[22] A. W. Ehlers, M. Boehme, S. Dapprich, A. Gobbi, A. Hoellwarth, V. Jonas, K. F. Koehler, R. Stegmann, A. Veldkamp, G. Frenking, Chem. Phys. Lett. 208 (1993) 111–114.

[23] A. Altomare, M. C. Burla, M. Camalli, G. L. Cascarano, C. Giacovazzo, A. Guagliardi, A. G. G. Moliterni, G. Polidori, R. Spagni, SIR97 a program for automatic solution of crystal structures by direct methods. J. Appl. Cryst. 32 (1999) 115–119.

[24] G. M. Sheldrick, Acta Cryst. A 64 (2008) 112-122.

[25] L. J. Farrugia, J. Appl. Cryst. 30 (1997) 565–566.

[26] M. R. Maurya, S. Agarwal, C. Bader, D. Rehder, Eur. J. Inorg. Chem. (2005) 147-157.

[27] D. F. Back, M. A. Ballin, G. Manzoni de Oliveira, J. Mol. Struct. 935 (2009) 151–155.

[28] (a) M. Ferrari Bellichi, G. Fava Gasparri, E. Leporati, C. Pelizzi, P. Tarasconi, G. Tosi, J. Chem. Soc., Dalton Trans. (1986) 2455–2462.

[29] J. S. Casas, E. E. Castellano, M. C. Rodríguez-Argüelles, A. Sánchez, J. Sordo, J. Zukerman-Schpector, Inorg, Chim. Acta 260 (1997) 183–188.

[30] D. Rehder, Transition Metal Nuclear Magnetic Resonance; Pregosin, P. S., Ed.; Elsevier: New York (1991) 1-58.

[31] M. R. Maurya, A. Kumar, A. R. Bhat, A. Azam, C. Bader, D. Rehder, Inorg. Chem. 45 (2006) 1260-1269.

[32] A. W. Addison, T. N. Rao, J. Reedijk, J. van Rijn, G. C. Verschoor, J. Chem. Soc. Dalton Trans. (1984) 1349-1356.

[33] C. Milsmann, Z. R. Turner, S. P. Semproni, P. J. Chirik, Angew. Chem. Int. Ed. Engl. 51 (2012) 5386-5390.

[34] P. I. D. Maia, V. M. Deflon, G. F. de Sousa, S. S. Lemos, A. A. Batista, O. R. Nascimento, E. Niquet, Z. Anorg. Allg. Chem. 633 (2007) 783-789.

[35] H. H. Monfared, S. Kheirabadi, N. A. Lalami, P. Mayer, Polyhedron 30 (2011) 1375–1384.

[36] H. Mimoun, I. Seree de Roch, L. Sajus, Tetrahedron 26 (1970) 37-50.

[37] K. B. Sharpless, J. M. Townsend, D. R. Williams, J. Am. Chem. Soc. 94 (1972) 295-296.

[38] (a) M. Bühl, R. Schurhammer, P. Imhof, J. Am. Chem. Soc. 126 (2004) 3310-3320. (b) G. Zampella, P. Fantucci, V. L. Pecoraro, L. De Gioia, J. Am. Chem. Soc. 127 (2005) 953-960. (c) Y. Nakagawa, N. Mizuno, Inorg. Chem. 46 (2007) 1727-1736. (d) A. E. Kuznetsov, Y. V. Geletii, C. L. Hill, K. Morokuma, D. G. Musaev, Inorg. Chem. 48 (2009) 1871-1878. (e) M. L. Kuznetsov, J. C. Pessoa, Dalton Trans. (2009) 5460-5468. (f) M. Vandichel, K. Leus, P. Van der Voort, M. Waroquier, V. Van Speybroeck, J. Catal. 294 (2012) 1-18.

[39] C. K. Sams, K. A. Jorgensen, Acta Chem. Scand. 49 (1995) 839-847.

[40] N. K. K. Raj, A. Ramaswamy, P. Manikandan, J. Mol. Catal. A 227 (2005) 37-45.

[41] (a) Y. D. Wu, D. K. W. Lai, J. Org. Chem., 60 (1995) 673-680. (b) D. Tantanak, M. A. Vincent, I. H. Hillier, Chem. Commun. (1998) 1031-1032. (c) I. V. Yudanov, P. Gisdakis, C. Di Valentin, N. Rosch, Eur. J. Inorg. Chem. (1999) 2135-2145.

[42] (a) F. E. Kühn, M. Groarke, E. Bencze, E. Herdtweck, A. Prazeres, A. M. Santos, M. J. Calhorda, C. C. Romão, I. S. Gonçalves, A. D. Lopes, M. Pillinger, Chem. Eur. J. 8 (2002) 2370-2383. (b) L. F. Veiros, A. Prazeres, P. J. Costa, C. C. Romão, F. E. Kühn, M. J. Calhorda, Dalton Trans. (2006) 1383-1389. (c) P. J. Costa, M. J. Calhorda, F. E. Kühn, Organometallics 29 (2010) 303-311. (d) A. Comas-Vives, A. Lledós, R. Poli, Chem. Eur. J., 16 (2010) 2147-2158.

[43] (a) C. Dinoi, M. Ciclosi, E. Manoury, L. Maron, L. Perrin, R. Poli, Chem. Eur. J. 16 (2010) 9572–9584. (b) C. Dinoi, R. Poli, L. Perrin, L. Maron, Dalton Trans. 41 (2012) 1131-1133.

[44] D. Balcells, F. Maseras, A. Lledós, J. Org. Chem. 68 (2003) 4265-4274.

[45] (a) A. Sarkar, S. Pal, Inorg. Chim. Acta 361 (2008) 2296-2304. (b) M. Cindrić, M. Rubčić, I. Đilović, G. Giester, B. Kamenar, Croat. Chem. Acta 80 (2007) 583-590. (c) W. Bansse, E.

Ludwig, E. Uhlemann, F. Weller, K. Dehnicke, W. Herrmann, Z. Anorg. Allg. Chem. 613 (1992) 36-44. (d) D. Wang, M. Ebel, C. Schulzke, C. Grüning, S. K. S. Hazari, D. Rehder, Eur. J. Inorg. Chem. (2001) 935-942. (e) M. Rubčić, D. Milić, G. Horvat, I. Đilovic, N. Galić, V. Tomišić, M. Cindrić, Dalton Trans. (2009) 9914–9923. (f) C. -T. Chen, J. -Q. Kao, S. B. Salunke, Y. -H. Lin, Org. Lett. 13 (2011) 26-29.